

# **AN IMPROVED METHOD FOR REAL-TIME AND ONLINE CORROSION MONITORING USING COUPLED MULTIELECTRODE ARRAY SENSORS**

Lietai Yang, Darrell S. Dunn and Gustavo A. Cragolino  
Center for Nuclear Waste Regulatory Analyses  
Southwest Research Institute®  
San Antonio, TX, U.S.A.

## **ABSTRACT**

Coupled multielectrode array sensors (MAS) may underestimate non-uniform corrosion rates in cases where the environment is not significantly corrosive because of possible internal electron flows on the most corroding electrode. An improved method was developed to derive the lower and upper bounding values for the non-uniform corrosion rate measured with the MAS probes. The lower boundary was measured when the electrodes of the MAS probe were at the natural coupling potential. The upper boundary was measured when the coupling potential of the MAS probe was raised to a value at which all electrodes are likely to be anodic. Under such raised coupling potential, possible internal electron flows within the most anodic electrode were stopped and their effects on the measured corrosion rate were eliminated.

Keywords: Multielectrode sensor, multielectrode probe, corrosion monitoring, corrosion sensor, localized corrosion sensor, online corrosion sensor, real-time corrosion sensor, coupled multiple electrodes.

## **INTRODUCTION**

Coupled multielectrode concept is one of the new developments in the past decade in the measurements of corrosion behaviors and studies of spatiotemporal patterns of electrochemical processes on metal surfaces.<sup>1-4</sup> Coupled multielectrode array sensors (MAS) give direct, one-parameter non-uniform corrosion rates derived from statistical parameters such as standard deviation of currents or most anodic current from the multiple electrodes. These sensors have made the quantitative real-time and online monitoring of non-uniform corrosion, especially localized corrosion such as pitting corrosion and crevice corrosion possible.<sup>5,6</sup> The MAS technology has been used successfully for online and real-time monitoring of corrosion in many different applications,<sup>7-26</sup> including in industrial chemical processes and cooling water systems.

A simple way to determine the quantitative penetration rate of localized corrosion using a MAS probe involves the assumption that there is no current that flows internally on the most corroding electrode.<sup>10</sup> This is a reasonable assumption if the metal is not corrosion resistant or if the environment

is highly corrosive. In these cases, a high probability exists that at least one or two of the probe electrodes will corrode severely. Under these conditions, no cathodic site is likely to exist on the most severely corroding electrode of the probe to accept current from the corroding sites on the same electrode. However, for a corrosion resistant alloy in a less corrosive environment, or for a metal in a corrosive environment during the early stages of corrosion when no electrode is more significantly corroded than the others in the probe, the assumption of zero internal current may underestimate the true localized corrosion penetration rate. This paper describes a new method that may be used to derive an upper bounding value for the penetration rate and thus reduce the uncertainty that may be caused by the internal current.

## THEORY

Figure 1 shows the working principle of the MAS probe.<sup>5,6,10</sup> The most anodic current\*, the current that flows through the external circuit from the most corroding electrode (or most anodic electrode) to the less corroding or non-corroding electrodes (cathodic electrodes) is usually used to derive the localized corrosion rate. The anodic current on the most corroding electrode corresponds to the highest corrosion rate or maximum penetration rate on a probe that simulates a metal coupon. Thus the corrosion rate from a MAS probe represents the highest penetration rate of localized corrosion (e.g., pitting corrosion) that may be found on a metal coupon.

Figure 2 shows the flow pattern of currents on the different kinds of electrodes in a coupled MAS probe. If the most anodic electrode in a given environment is not the totally corroded active electrode (Figure 2a), but is a partially corroded electrode (Figure 2b), it would still have cathodic sites to accept electrons from the neighboring anodic sites<sup>6,10</sup> on the same anode. The total anodic current or corrosion current,  $I_a$ , is the sum of the external anodic current,  $I_a^{ex}$ , and the internal anodic current that flows from the cathodic sites within the electrode,  $I_a^{in}$ :

$$I_a = I_a^{ex} + I_a^{in} \quad (1)$$

The coupled MAS probe relies on the measurement of the external anodic current to estimate the non-uniform corrosion rate according to Eq. (1). As  $I_a^{in}$  is not measurable, the corrosion current may also be expressed as<sup>10</sup>

$$I_a = I_a^{ex} / \varepsilon \quad (2)$$

Where  $\varepsilon$  is a current distribution factor ( $0 < \varepsilon \leq 1$ ) that represents the fraction of electrons that flow to other electrodes through the external circuit (Figures 1 and 2). In Figure 2a, the anode is a totally active and corroded electrode. All or most of its corrosion electrons flow to the other electrodes through the external circuit, and the corresponding  $\varepsilon$  would be equal or close to unity. On the other hand, in Figure 2b, the anode is a partially corroded electrode, a portion of its corrosion electrons flow to the local cathodic sites, and the corresponding  $\varepsilon$  is less than 1. Therefore, in the case of Figure 2b there is uncertainty with using the coupled MAS probe to predict the corrosion rate assuming  $\varepsilon = 1$ .

Localized corrosion processes include nucleation of metastable pits, stabilization of these pits, and, if conditions permit, repassivation of stable pits. A number of factors support the nucleation of metastable pits, but it is well recognized that the anodic dissolution processes occurring in the pit nuclei create a local acidification through the hydrolysis of dissolved metal cations.<sup>27,28</sup> The acidification and generation of increasing concentrations of metal cations and the migration of anions to the pits lead to the precipitation of a metal-anion salt film inside the pits.<sup>29,30</sup> The various contributions to the current in

---

\* The statistical equivalents of the most anodic current, such as the value of mean current plus 2.5 or 3 times the standard deviation of the currents from the different electrodes or the value of the 95<sup>th</sup> percentile of anodic currents from the different electrodes were also used<sup>10</sup>. To simplify the discussion, this paper will focus on the use of the most anodic current to derive the corrosion rate.

the case of the MAS probe in a typical localized corrosion environment are shown schematically in Figure 3. At the anodic areas, metal cations are generated as shown in Eqs. (3) through (5) for the case of a Fe-Cr-Ni alloy,



The dissolution of a cathodic electrode in the MAS probe, particularly the most cathodic electrode, may be in the passive regime as shown in Figure 3 by the upper anodic curve (Curve I). On the other hand, the dissolution of an anode in the MAS probe, particularly the most anodic electrode, may be in the active regime. For the active electrode, the dissolution process inside the pits can be a mixture of active dissolution, ohmic controlled dissolution, and transport controlled dissolution, depending on the potential regime, time of active pit growth, size of pits, and external electrolyte composition.<sup>31</sup> This is indicated schematically in Figure 3 by the lower anodic curve (Curve II). This anodic dissolution curve is the behavior of the alloy in the pit electrolyte, not in the external electrolyte.

At the cathodic areas, the electrons are consumed by the cathodic half-cell reactions represented simplistically by Eqs. (6–8),



The composite rate of the reduction reactions for the oxygen, proton or other species is represented in Figure 3 by the cathodic curve (Curve III). For the cathode exhibiting passive dissolution, the open-circuit potential (when not coupled with the other electrodes),  $E_{ca}$ , is a mixed potential that is determined by the intersection of the cathodic curve with the upper anodic curve (Figure 3). For the most anodic electrode exhibiting active pitting, the corrosion potential,  $E_{an}$ , is determined by the intersection of the cathodic curve with the lower anodic curve (Figure 3).

Figures 4 and 5 show some typical open-circuit potentials measured from the individual electrodes in two coupled MAS probes in a 0.5 M NaCl solution. Because the solution was not corrosive enough to cause significant localized corrosion for the probe alloys (Alloy 276 and Type 316 stainless steel) (see the Example Results section), none of the electrodes exhibited active pitting potential (low potential). These figures, however, demonstrate that there is a significant difference between the most anodic electrode and the most cathodic electrode (60 to 150 mV) in the coupled MAS probes. The most anodic electrode used to derive the penetration rate in a coupled MAS probe is the electrode that gives the largest anodic current during coupling and it is usually the one that gives the lowest open-circuit potential at the instance the electrodes are decoupled. Similarly, the most cathodic electrode is the electrode that gives highest cathodic current during coupling, and it is usually the one that gives the highest open-circuit potential. At different times, the most anodic or the most cathodic electrode may not be the same electrodes because of changes in conditions at each electrode over time.

When the electrodes are coupled, the potential of the probe electrodes,  $E_{coup}$ , is given by the potential at which the net current for all the electrodes in the probe sums to zero:

$$\sum (i_p \times A_p) + \sum (i_a \times A_a) = \sum (i_c \times A_c) \quad (9)$$

where,  $i_p$ ,  $i_a$ , and  $i_c$  are the current densities of passive, active, and cathodic processes respectively, and  $A_p$ ,  $A_a$ , and  $A_c$  are the corresponding areas. The coupling potential,  $E_{coup}$ , determines whether an electrode in a MAS probe or a reaction site on an electrode is anodic or cathodic.

## NEW APPROACH

As discussed previously, the coupling potential,  $E_{\text{coup}}$ , determines whether an electrode in a MAS probe or a reaction site on an electrode is anodic or cathodic. If the most anodic electrode is totally corroded (or totally active) (Figure 2a), the potential of all the sites on the electrode would be lower than  $E_{\text{coup}}$  and therefore there is no internal current ( $I_a^{\text{in}} = 0$ ). If, however, the most anodic electrode is only partially corroded (Figure 2b), some reaction sites on the electrode may have a potential that is higher than  $E_{\text{coup}}$ , and therefore there is an internal current ( $I_a^{\text{in}} \neq 0$ ).

It should be noted that, the ratio of the cathodic surface area to the active surface area must be large enough to have a significant  $I_a^{\text{in}}$  because the cathodic areas are usually under passive state with a low current density.

In a MAS probe, the multiple electrodes simulate the different cathodic and anodic sites of a metal coupon. If the number of electrodes is large and the size of the electrodes is sufficiently small, the highest potential (usually the potential measured from the most cathodic electrode) can be considered to statistically represent the potential of the most cathodic site on the metal (after it is electrically isolated from the other sections of the metal). The potential measured from the most cathodic electrode may also be considered as the highest bounding potential for all the cathodic sites, if they exist, on the most anodic electrode. Therefore, if the coupling potential of the MAS probe is raised to a value ( $E'_{\text{coup}}$  in Figure 3) that is slightly higher than the potential measured from the most cathodic electrode, there should be no cathodic reaction on the most anodic electrodes, even though some areas are still uncorroded. Under this condition,  $\varepsilon \rightarrow 1$  and  $I_a^{\text{in}} \rightarrow 0$  [Eqs. (1) and (2)], the uncertainty in the measured corrosion rate from the coupled MAS probe due to  $I_a^{\text{in}}$  can be eliminated.

In Figure 6, a polarization unit is incorporated in a coupled MAS probe instrument to dynamically adjust the potential of the coupling joint of the probe such that the currents from the most cathodic electrode of the MAS probe is slightly anodic (less than zero if an anodic current is recorded as a negative current by the instrument or larger than zero if a cathodic current is recorded as a negative current by the instrument). Under this condition, the open-circuit potential of the most cathodic electrode is lower than the coupling potential. In practice, the coupling potential may also be raised according to other criteria determined on the basis of statistical analysis. For example, it may be raised to a value at which 99% of the reaction sites on the most cathodic electrode are likely to be anodic. Because the coupling potential is adjusted based on the current from the most anodic electrode or from its statistical equivalent, no additional reference electrode is required.

Raising the coupling potential also increases the current from the active sites. The corrosion rate measured at the raised coupling potential may be higher than the actual corrosion rate. Thus the corrosion rate measured at the raised coupling potential,  $E'_{\text{coup}}$ , may be considered as the upper bounding corrosion rate. The corrosion rate measured under the natural coupling potential,  $E_{\text{coup}}$ , may be considered as the lower bounding corrosion rate because of the possible non-zero internal flow of electrons on the most corroding electrode at this potential. This upper bounding value is not an unrealistic overestimate because the raised coupling potential is an actual value measured from one of the electrodes made of the same material. It is possible for the potential around a small pit to be at the raised coupling potential if it is surrounded by a large passive area. On the other hand, the active sites are usually covered by corrosion products and therefore the dissolution is under ohmic and mass-transport controlled dissolution. The increase in measured corrosion rate with the increased coupling potential due to the contribution from the active sites may be limited (see Curve II in Figure 3).

## EXAMPLE RESULTS

In the absence of an integrated instrument (Figure 6) that measures the signals from the MAS probe and, at the same time, dynamically adjusts the coupling potential based on the measured signals,

a regular multielectrode system<sup>10</sup> and a multichannel potentiostat (Solartron MultiStat-1480) were used for the demonstration experiment. In this experiment, three MAS probes made of Alloy 276, Type 316 stainless steel and Type 1008 carbon steel were tested in separate electrochemical cells filled with an air-saturated 0.5 M NaCl solution. All the three probes had eight electrodes. The regular system for the MAS probes was used to continuously measure the signals from the MAS probes, and the potentiostat was used to independently control the potential of the coupling joints of the different probes. Figure 7 shows the pattern of potential applied to the coupling joint of the MAS probes by the potentiostat. The potential scanning rate was  $\pm 0.008$  mV/sec.

Figure 8 shows typical responses of the currents from the Alloy 276 probe to the changes in potential in a 0.5 M NaCl solution at room temperature. In Figure 8, the currents are the outputs from the multielectrode sensor system; the negative currents are anodic currents and the positive currents are cathodic currents. When the coupling joint was not polarized (i.e., at its open-circuit potential), the MAS probe was used as before.<sup>10</sup> During the anodic scan, when the potential reached  $E'_{\text{coup}}$  (approximately  $0.025 V_{\text{SCE}}$ ), all the currents became anodic. On the other hand, during the cathodic scan, when the potential reached approximately  $0.05 V_{\text{SCE}}$ , all the currents became cathodic and no electrode was corroding.

Figures 9, 10 and 11 show typical responses of the currents from the three probes (Alloy 276, Type 316 stainless steel, and Type 1008 carbon steel) to the changes in potential during the start of anodic scan after the probes were at their natural coupling potential,  $E_{\text{coup}}$ . The absolute value of the current from the most anodic electrode for each probe (Electrode #5 in Figure 9, #6 in Figure 10 and #8 in Figure 11) increased with the increase in potential and reached  $I_a'$  at  $E'_{\text{coup}}$ . In Figure 11, the open-circuit potential (when it was not coupled to the other electrodes of the MAS probe) and polarization behavior of one electrode (Electrode #7) was statistically abnormal and gave exceptionally high open-circuit potential and cathodic currents. This abnormal behavior may be caused by the contamination of that electrode by some metal particles introduced during the fabrication or polishing processes that are more noble than the carbon steel material. Therefore, Electrode #7 was excluded from the analysis and was not shown in Figure 11.

Figures 12, 13 and 14 show the corresponding responses of corrosion rates to the changes in potential. In Figures 12, 13 and 14, the corrosion rate from each probe was derived based on the current from its most anodic electrode at the natural coupling potential (before the potential scan was started). As discussed in the previous section, for each probe, the corrosion rate measured at  $E'_{\text{coup}}$  is the upper bounding value and the corrosion rate measured at  $E_{\text{coup}}$  is the lower bounding value. The lower and upper corrosion rate bounding values are denoted as  $r$  and  $r'$ , respectively, and are given in Table 1 for the different MAS probes. The lower-to-upper ratios for the bounding non-uniform corrosion values are from 2.2 to 2.7. Under localized corrosion conditions, the penetration rates usually vary by orders of magnitude from coupon to coupon in the same solution, and even vary from location to location on the same coupon. These ranges of bounding values are quite narrow compared to the variations in penetration rate for non-uniform corrosions. Therefore, the improved method provides an excellent way to measure and derive a quantitative corrosion rate in a localized corrosion environment.

In addition, as discussed in the Theory section, Figures 4 and 5 show that none of the electrodes in the Alloy 276 and Type 316 stainless steel MAS probes exhibit active dissolution. Indeed, the rates obtained from these probes (Figures 12 and 13, and Table 1) are low,  $<0.64 \mu\text{m}/\text{year}$  for Alloy 276 and  $<2.2 \mu\text{m}/\text{year}$  for the Type 316 stainless steel.

The non-uniform corrosion rate from the Type 1008 carbon steel MAS (Figure 14) probe was high, between  $229$  and  $543 \mu\text{m}/\text{year}$ . This measured high corrosion rate is consistent with the low  $E_{\text{coup}}$  value ( $-0.641 V_{\text{SCE}}$ ) that simulates the open-circuit potential of a coupon, and indicates that the metal was under active dissolution conditions.

In the derivation of the corrosion rate for each probe, the current from the electrode that was the most anodic under the natural coupling potential,  $E_{\text{coup}}$ , was used. However, during the potential scan or after the coupling potential was raised, another electrode may become the electrode that gives the most anodic current. For example, Electrode #4 in Figure 9 became the most anodic electrodes shortly after the potential scan. An alternative way to determine the corrosion rate for each probe may be to use the current from the electrode that is the most anodic at the raised coupling potential. In the same manner used to derive the corrosion rates at natural coupling potentials<sup>10</sup>, a statistically derived most anodic current that uses the information from all of the anodic electrodes may reduce the uncertainty. Examples of the statistical equivalents of the most anodic current include the 95<sup>th</sup> percentile of the anodic currents, or the mean plus three times the standard deviation of the anodic currents flowing through all electrodes in the coupled MAS probe at the raised coupling potential.

## CONCLUSIONS

An improved method was derived to obtain the lower and upper bounding values for the non-uniform corrosion rate measured with coupled multielectrode array sensor (MAS) probes. The lower boundary was measured using standard methods when the electrodes of the MAS probe were at the natural coupling potential. The upper boundary was measured when the coupling potential of the MAS probe was raised to a value at which all possible cathodic sites on the most anodic electrodes statistically became anodic. Under such raised coupling potential, all possible internal electron flows within the most anodic electrode were stopped and their effects on the measured corrosion rate were eliminated. For the probes made of Alloy 276, Type 316 stainless steel and type 1008 carbon steel in a 0.5 M NaCl solution, the upper bounds were found to be 2.2 to 2.7 times the lower bounds.

## ACKNOWLEDGEMENTS

The work reported in this paper was funded by the Southwest Research Institute Internal Research and Development Program. Technical discussions with N. Sridhar, Vijay Jain and English Percy, and the laboratory assistance of Brian Derby are acknowledged. The authors would like to thank the technical review of Y.-M. Pan, the programmatic review of D. Turner, and the assistance of J. Gonzalez and L. Selvey in preparing this paper.

## REFERENCES

1. U. Steinsmo, T. Rone, and J.M. Drugli, Aspects of Testing and Selecting Stainless Steels for Sea Water Applications, CORROSION/94, Paper No. 492, Houston, TX: NACE International, 1994.
2. Z. Fei, R.G. Kelly, and J.L. Hudson, Journal of Physical Chemistry, 100(49), pp. 18,986-18,991, 1996.
3. Y.J. Tan, Corrosion Science, 41(2), pp. 229-247, 1999.
4. Y. J. Tan, T. Liu and N. Aung, Localized Corrosion and Inhibition Studies Using the Wire Beam Electrode Method in Conjunction with the Electrochemical Noise Analysis and the Scanning Reference Electrode Technique, CORROSION/2004, Paper No. 04427, Houston, TX: NACE International, 2004.
5. L. Yang and N. Sridhar, Monitoring of Localized Corrosion, ASM Handbook, Volume 13A-Corrosion: Fundamentals, Testing, and Protection, Stephen. D. Crammer and Bernard S. Covino, Jr., eds, Materials Park, OH: ASM International, pp. 519-524, 2003.

6. L. Yang and N. Sridhar, *Materials Performance*, 42(9), pp. 48-52, 2003.
7. L. Yang, N. Sridhar, and O. Pensado, Development of a Multielectrode Array Sensor for Monitoring Localized Corrosion, Presented at the 199th Meeting of the Electrochemical Society, Abstract #182, Extended Abstract Volume I, 2001.
8. L. Yang, and D. S. Dunn, Evaluation of Corrosion Inhibitors in Cooling Water Systems Using a Coupled Multielectrode Array Sensor, CORROSION/2002, Paper No. 02004, Houston, TX: NACE International, 2002.
9. L. Yang, N. Sridhar, and G. Cragolino, Comparison of Localized Corrosion of Fe-Ni-Cr-Mo Alloys in Concentrated Brine Solutions Using a Coupled Multielectrode Array Sensor, NACE Corrosion/2002, Paper No. 545, NACE International, 2002.
10. L. Yang, N. Sridhar, O. Pensado, and D. S. Dunn, *Corrosion*, 58, p. 1,004, 2002.
11. C. Sean Brossia and Lietai Yang, Studies of Microbiologically Influenced Corrosion Using a Coupled Multielectrode Array Sensor, CORROSION/2003, Paper No. 03575, Houston, TX: NACE International, 2003.
12. C.S. Brossia, L. Yang, D.S. Dunn, N. Sridhar, Corrosion Sensing and Monitoring, Proceedings of Tri-Service Corrosion Conference, January 14-18, 2002, San Antonio, TX, 2002.
13. V. Jain, S. Brossia, D. Dunn, and L. Yang, Development of Sensors for Waste Package Testing and Monitoring in the Long Term Repository Environments, *Ceramic Transactions Vol. 143*, Westerville, OH: American Ceramic Society, pp. 283-290, 2003.
14. L. Yang, R.T. Pabalan, L. Browning, and D.S. Dunn, Corrosion Behavior of Carbon Steel and Stainless Steel Materials Under Salt Deposits in Simulated Dry Repository Environments, *Scientific Basis for Nuclear Waste Management XXVI, Symposium Proceedings 757R*, J. Finch and D. B. Bullen, eds, Warrendale, PA: Materials Research Society, pp. 791-797, 2003.
15. L. Yang, R. T. Pabalan, L. Browning, and G. A. Cragolino, Measurement of Corrosion in Saturated Solutions Under Salt Deposits Using Coupled Multielectrode Array Sensors, CORROSION/2003, Paper No. 03426, Houston, TX: NACE International, 2003.
16. A. Anderko, N. Sridhar, C. S. Brossia, D. S. Dunn, L.T. Yang, B.J. Saldanha, S.L. Grise, and M.H. Dorsey, An Electrochemical Approach to Predicting and Monitoring Localized Corrosion in Chemical Process Streams, CORROSION/2003, Paper No. 03375, (Houston, TX: NACE International, 2003). Figures 18-20
17. L. Yang, R.T. Pabalan, and D.S. Dunn, The Study of Atmospheric Corrosion of Carbon Steel and Aluminum under Salt Deposit Using Coupled Multielectrode Array Sensors, the 204th Meeting of the Electrochemical Society, Abstract #465, Extended Abstract Volume, 2003-II.
18. M. H. Dorsey, L. Yang and N. Sridhar, Cooling Water Monitoring Using Coupled Multielectrode Array Sensors and Other On-line Tools, CORROSION/2004, Paper No. 04077, Houston, TX: NACE International, 2004.
19. L. Yang, N. Sridhar, S.L. Grise, B.J. Saldanha, M.H. Dorsey, H.J. Shore, and A. Smith, Real-Time Corrosion Monitoring in a Process Stream of a Chemical Plant Using Coupled Multielectrode Array Sensors, CORROSION/2004, Paper No. 04440, Houston, TX: NACE International, 2004.

20. L. Yang, N. Sridhar, D.S. Dunn, and C.S. Brossia, Laboratory Comparison of Coupled Multielectrode Array Sensors with Electrochemical Noise Sensors for Real-Time Corrosion Monitoring, CORROSION/2004, Paper No. 04033, Houston, TX: NACE International, 2004.
21. X. Sun, Online Monitoring of Undercoating Corrosions Utilizing Coupled Multielectrode Sensors, CORROSION/2004, Paper No. 04033, Houston, TX: NACE International, 2004.
22. X. Sun, Online Monitoring of Corrosion under Cathodic Protection Conditions Utilizing Coupled Multielectrode Sensors, CORROSION/2004, Paper No. 04094, Houston, TX: NACE International, 2004.
23. L. Yang, N. Sridhar, C.S. Brossia, and D.S. Dunn, Evaluation of the Coupled Multielectrode Array Sensor as a Real Time Corrosion Monitor, Corrosion Science, Accepted for publication, 2004.
24. L. Yang and N. Sridhar, Sensor Array and Method for Electrochemical Corrosion Monitoring, U.S. Patent No. 6,683,463 (2004).
25. L. Yang, D. S. Dun and G. A. Cragnolino, An Improved Method for Real-time and Online Corrosion Monitoring Using Coupled Multielectrode Array Sensors, CORROSION/2005, Paper No. 05379, Houston, TX: NACE International, 2005.
26. L. Yang and G. A. Cragnolino, Studies on The Corrosion Behavior of Stainless Steels in Chloride Solutions in the Presence of Sulfate Reducing Bacteria, CORROSION/2004, Paper No. 04598, Houston, TX: NACE International, 2004.
27. G.T. Burstein and S.P. Mattin, Philosophical Magazine Letters 66, p. 127, 1992.
28. P.C. Pistorius and G.T. Burstein, Philosophical Transactions of The Royal Society of London A 341, p. 531, 1992.
29. H.S. Isaacs, J. of Electrochem. Soc., 120, p. 1,456, 1973.
30. N. Sridhar, D.S. Dunn, C.S. Brossia and G.A. Cragnolino, Stabilization and Repassivation of Localized Corrosion, Localized Corrosion, Research Topical Symposium, G.S. Frankel and J.R. Scully, eds, Houston, TX: NACE International, pp. 1-29, 2001.
31. H. Boehni and F. Hunkeler, Growth Kinetics and Stability of Localized Corrosion Processes, Advances in Localized Corrosion, H.S. Isaacs, U. Bertocci, J. Kuger, and S. Smialowska, eds, Houston, TX: NACE International, p. 69, 1990.

TABLE 1  
BOUNDING VALUES OF THE NON-UNIFORM CORROSION RATES MEASURED FROM THE  
DIFFERENT PROBES WITH THE IMPROVED METHOD ( $\mu\text{m}/\text{YEAR}$ )

Probes	Lower Bounding Value	Upper Bounding Value	Upper-To-Lower Bound Ratio
Alloy 276	0.240	0.640	2.67
Type 316 stainless steel	1.00	2.15	2.20
Type 1008 carbon steel	229	543	2.37

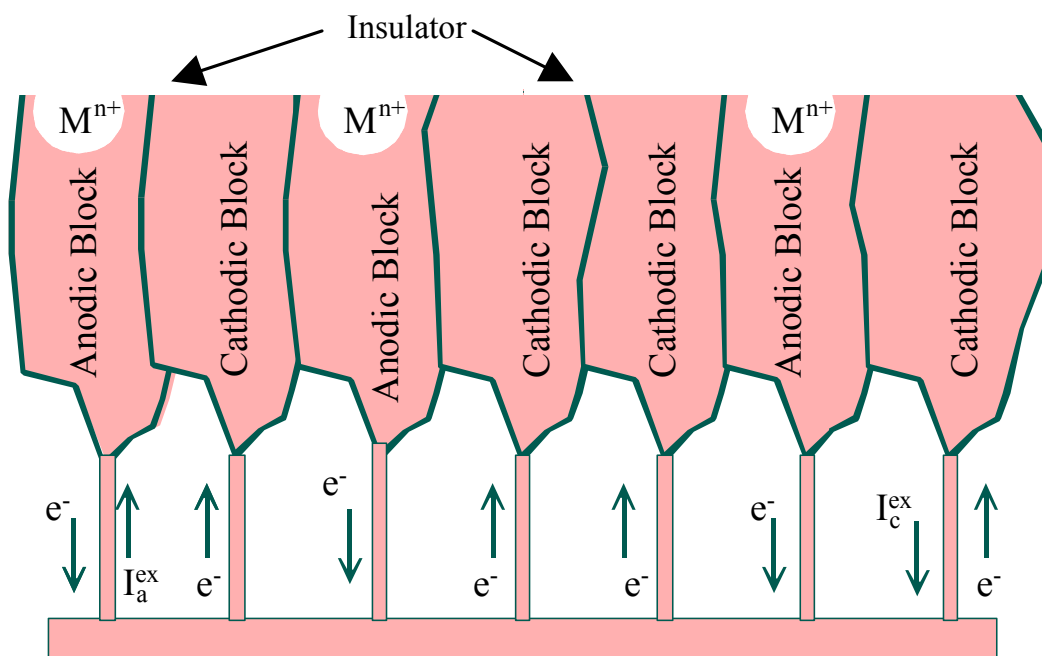


FIGURE 1. Flows of electrons and currents among electrically isolated cathodic and anodic blocks on the surface of a corroding metal under localized corrosion conditions.  $I_a^{ex}$  and  $I_c^{ex}$  are the external anodic and cathodic currents, respectively.

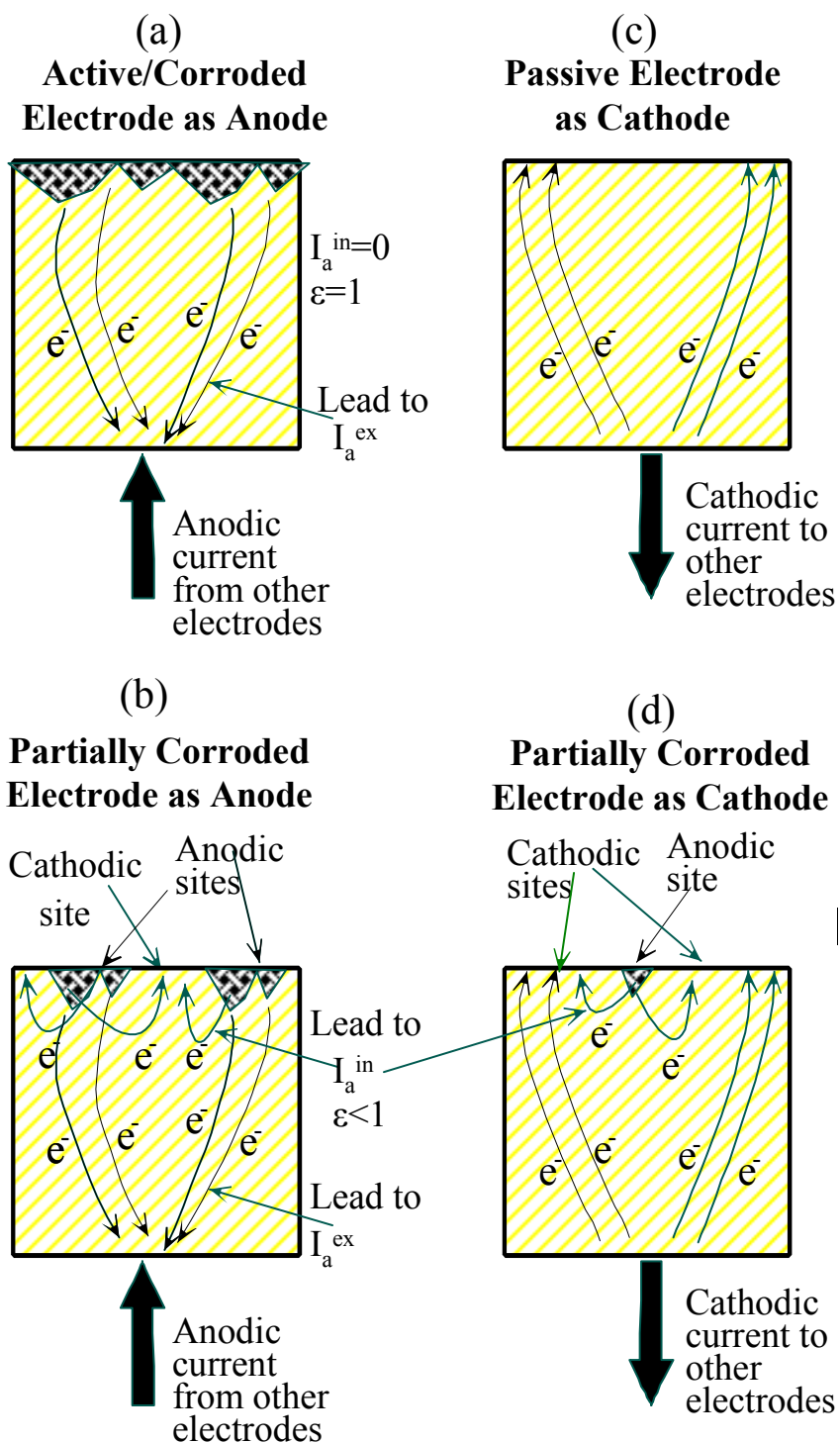


FIGURE 2. Flow of electrons on a totally corroded active electrode as anode (a), a partially corroded electrode as anode (b), a passive electrode as cathode (c), and a partially corroded electrode as cathode (d) in a coupled MAS probe.

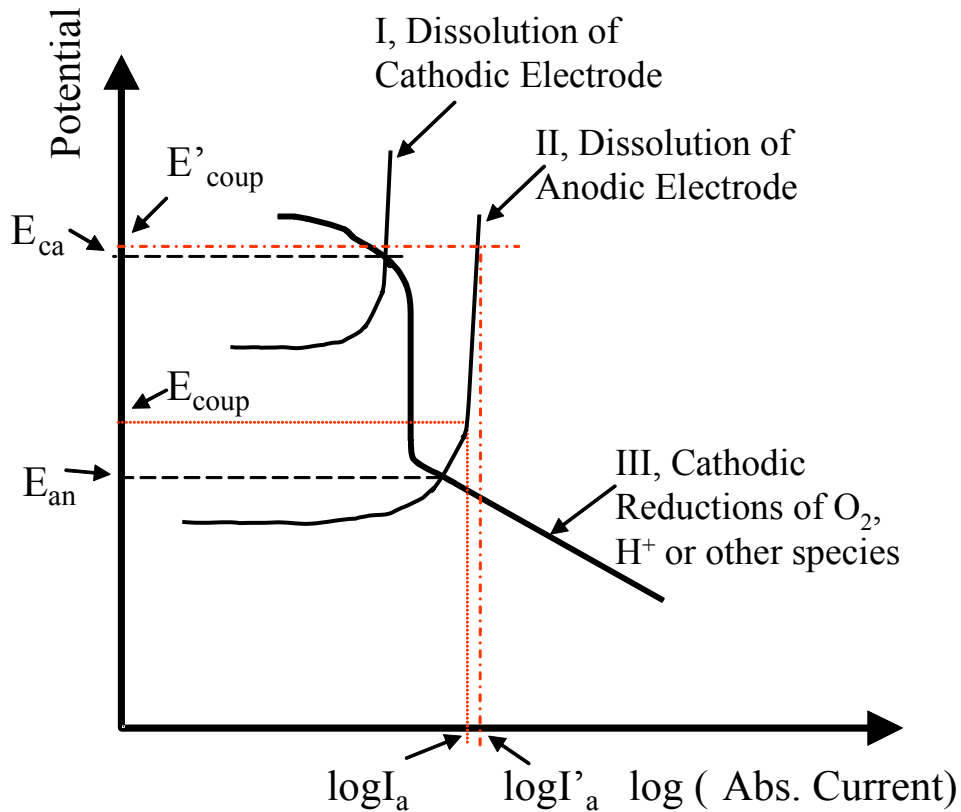


FIGURE 3. Schematic diagram of open-circuit electrode potentials for a cathodic electrode and an anodic anode, the natural and raised coupling potentials, and the dissolution currents of the anodic electrode at different coupling potentials in a MAS probe.

Note: The natural coupling potential,  $E_{\text{coup}}$ , simulates the corrosion potential of a piece of metal that has both active and passive sites on it. The raised coupling potential,  $E'_{\text{coup}}$ , is the potential equal or above the potential of the most cathodic electrodes.

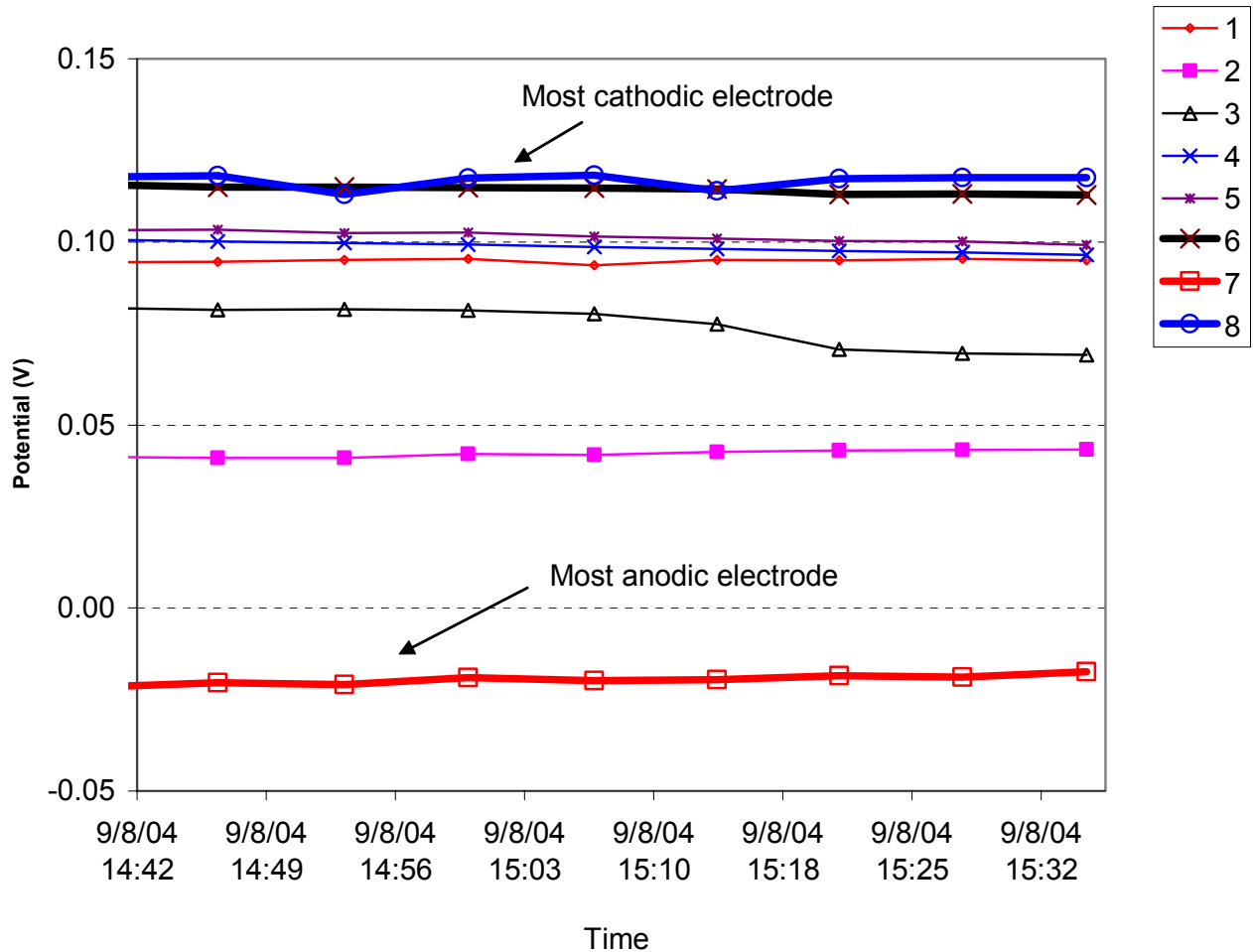


FIGURE 4. Typical open-circuit potentials measured from a coupled MAS probe made of Alloy 276 in a 0.5 M NaCl solution.

Note: The number in the legend denotes the identification number of the electrodes in the probe. The most anodic electrode under open-circuit condition was Electrode #7. The most cathodic electrode under open-circuit condition was either Electrode #8 or Electrode #6.

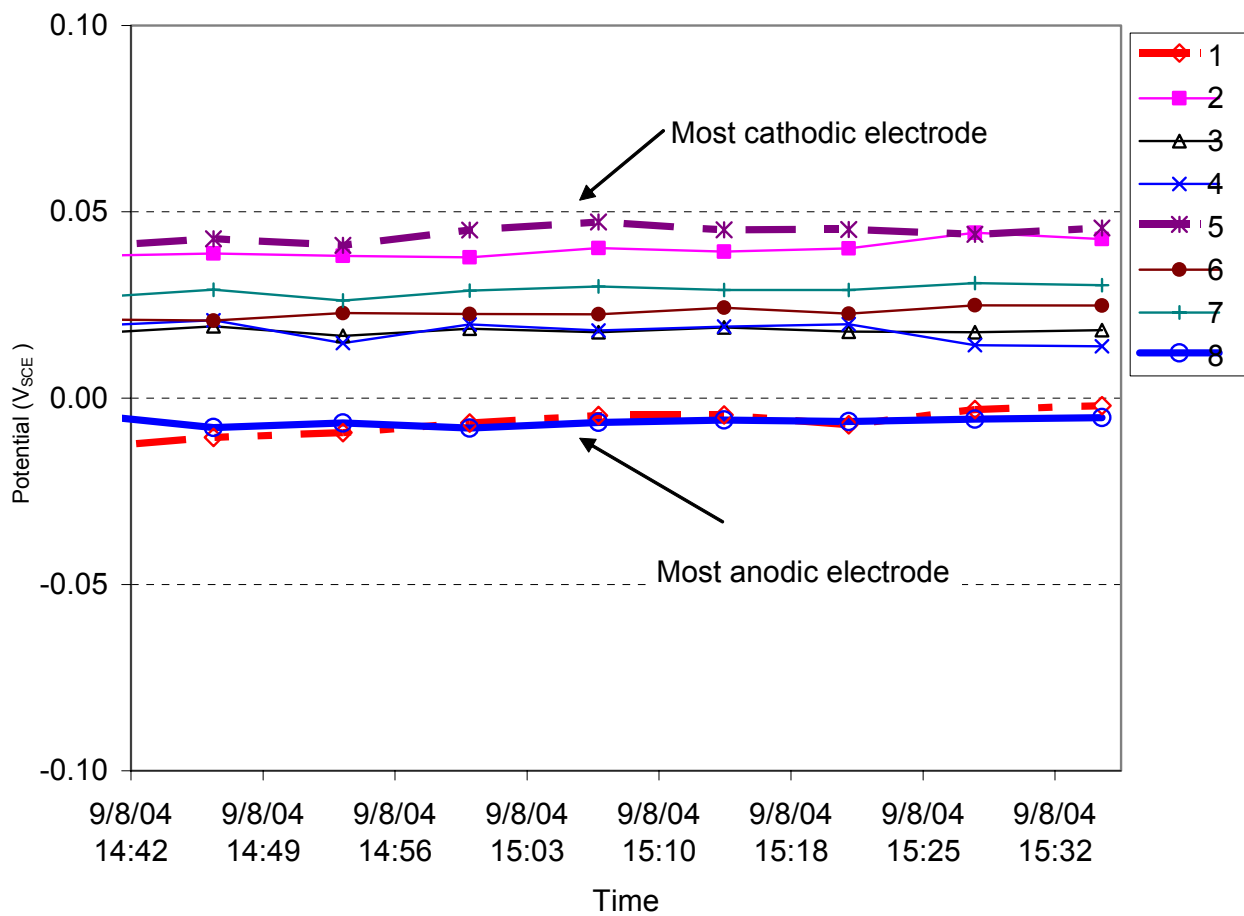


FIGURE 5. Typical open-circuit potentials measured from a coupled MAS probe made of Type 316 stainless steel in a 0.5 M NaCl solution

Note: The number in the legend denotes the identification number of the electrodes in the probe. The most anodic electrode under open-circuit condition was either Electrode #8 or Electrode #1. The most cathodic electrode under open-circuit condition was Electrode #5

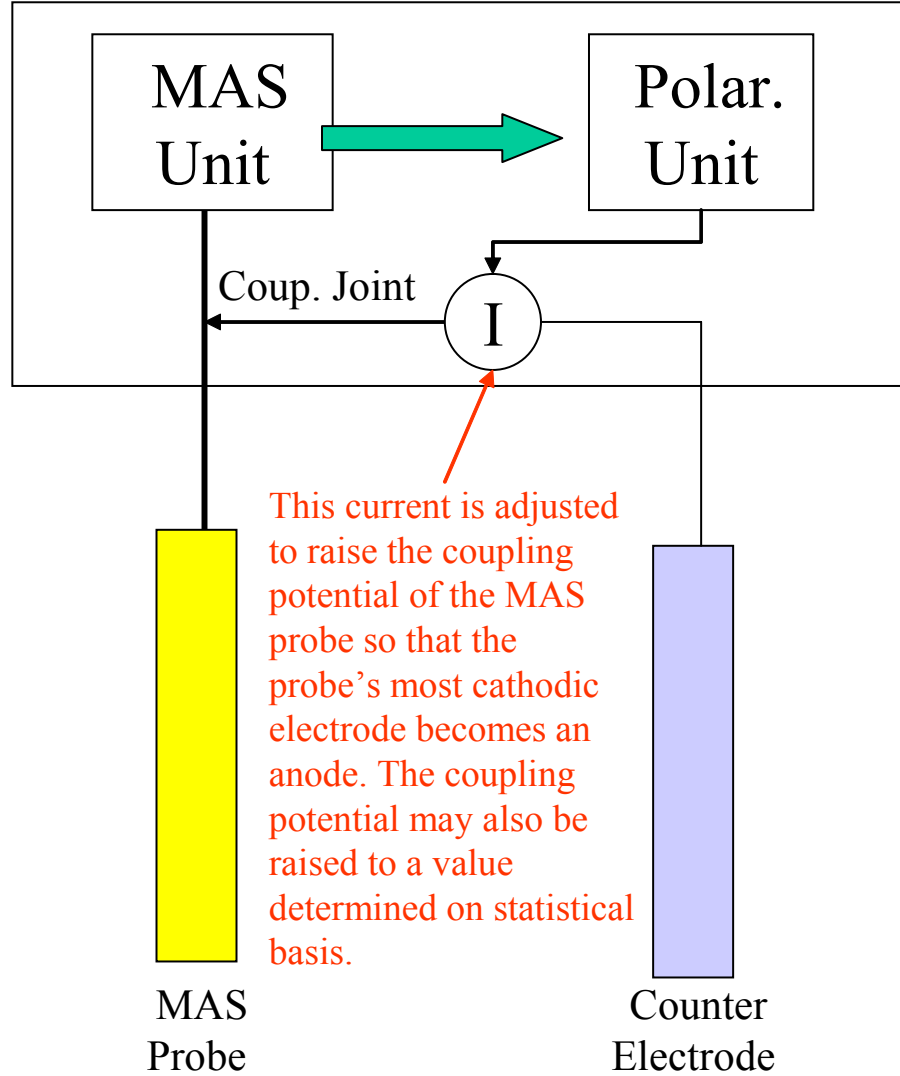


FIGURE 6. A proposed system that measures the corrosion rate using a coupled MAS probe at a raised coupling potential

Patent pending.

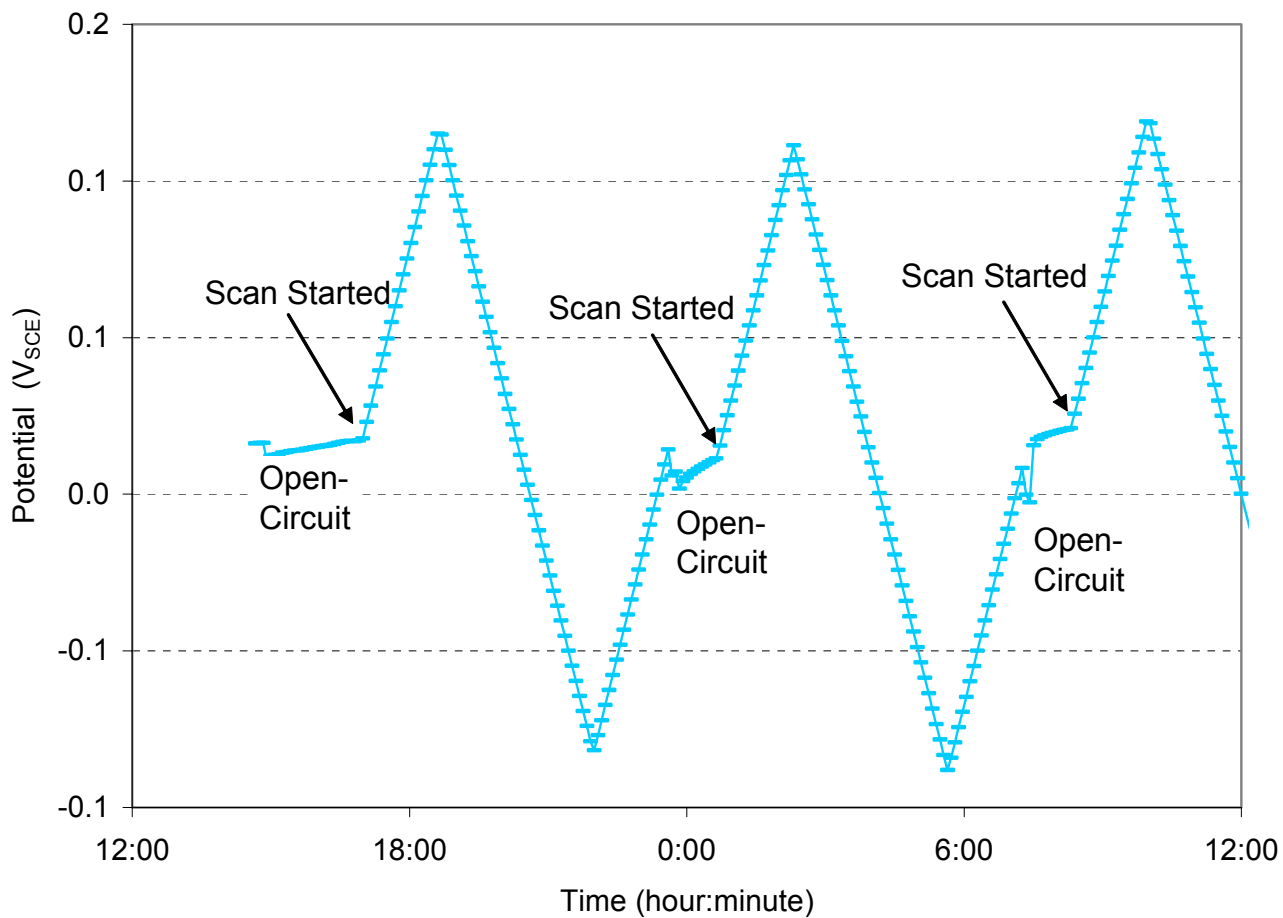


FIGURE 7. Potential applied by a potentiostat to the coupling joint of the MAS probes during a preliminary demonstration test using the improved method

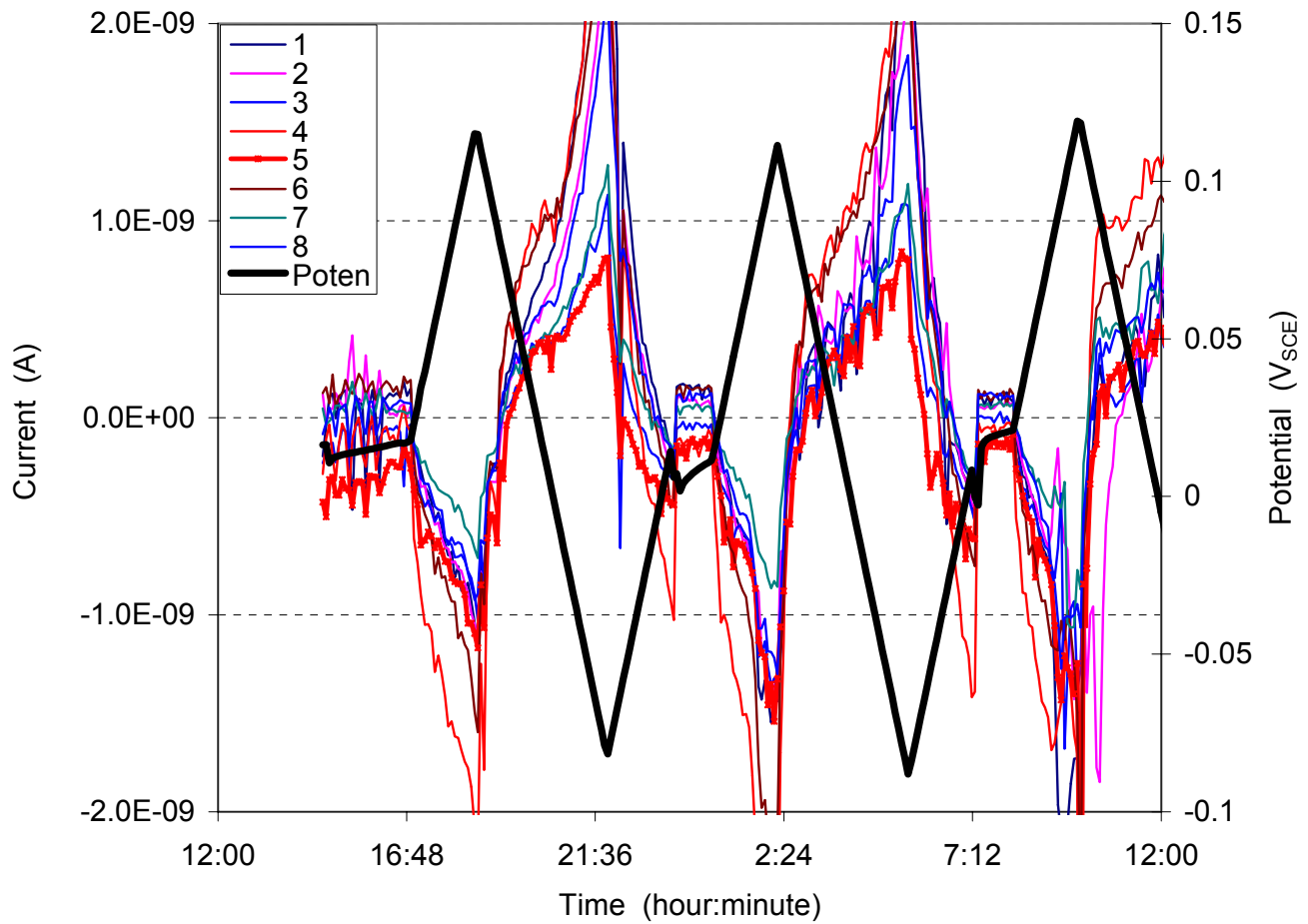


FIGURE 8. Responses of the currents from an eight-electrode MAS probe made of Alloy 276 to the potential changes as shown in Figure 7 in a 0.5 M NaCl solution

Note: Negative currents are anodic currents and positive currents are cathodic currents. The numbers in the legend are the identification numbers of the electrodes in the probe. Electrode #5 was the most anodic electrode at natural coupling potentials during the test.

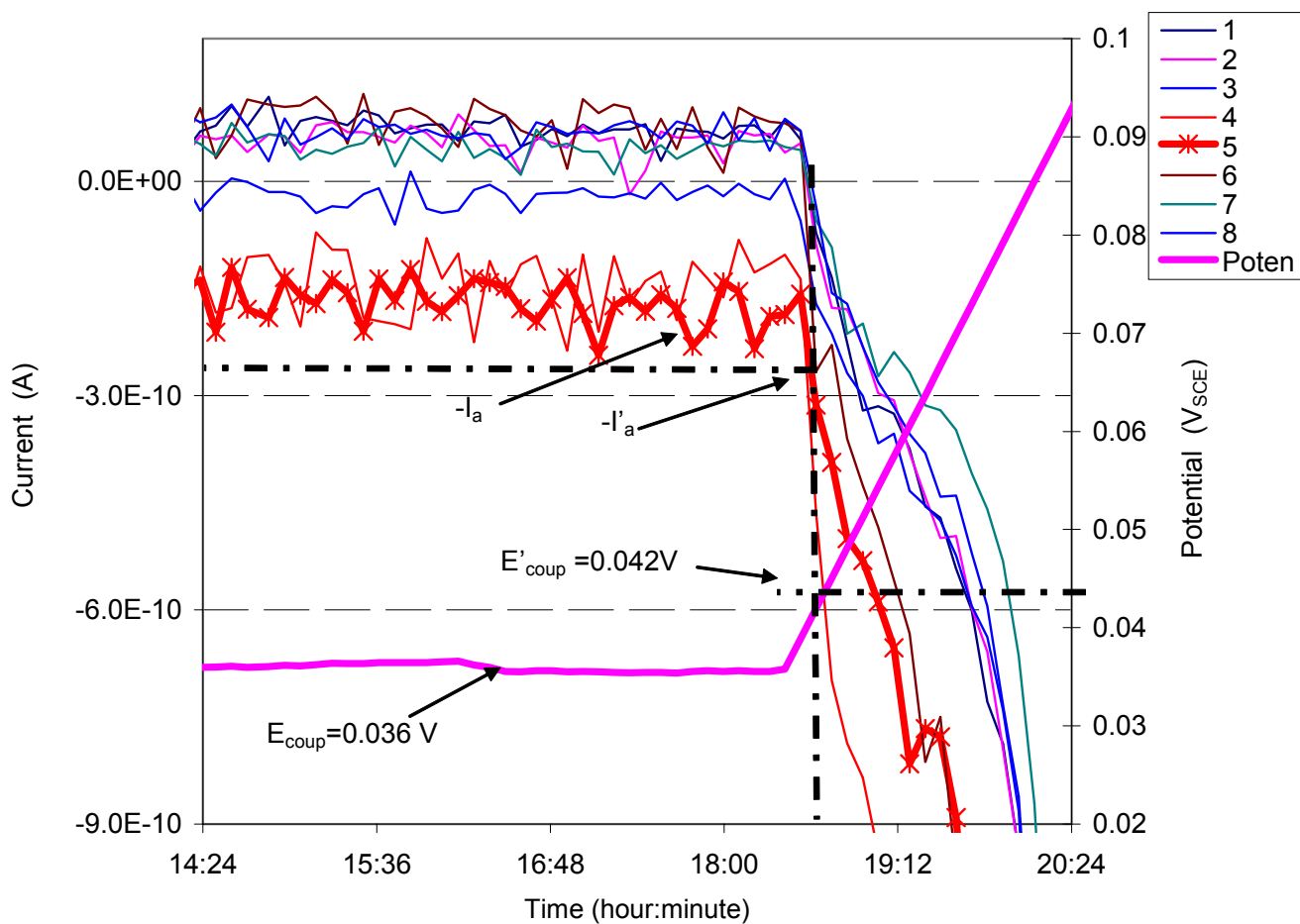


FIGURE 9. Response of the currents from the different electrodes in an Alloy 276 MAS probe to the anodic potential scan in a 0.5 M NaCl solution

Note: Negative currents are anodic currents and positive currents are cathodic currents. The numbers in the legend denotes the identification numbers of the electrodes in the probe. Electrode #5 was the most anodic electrode before the potential scan (at the natural coupling potential,  $E_{\text{coup}}$ ). Electrode #4 was the most anodic electrode shortly after the potential scan.

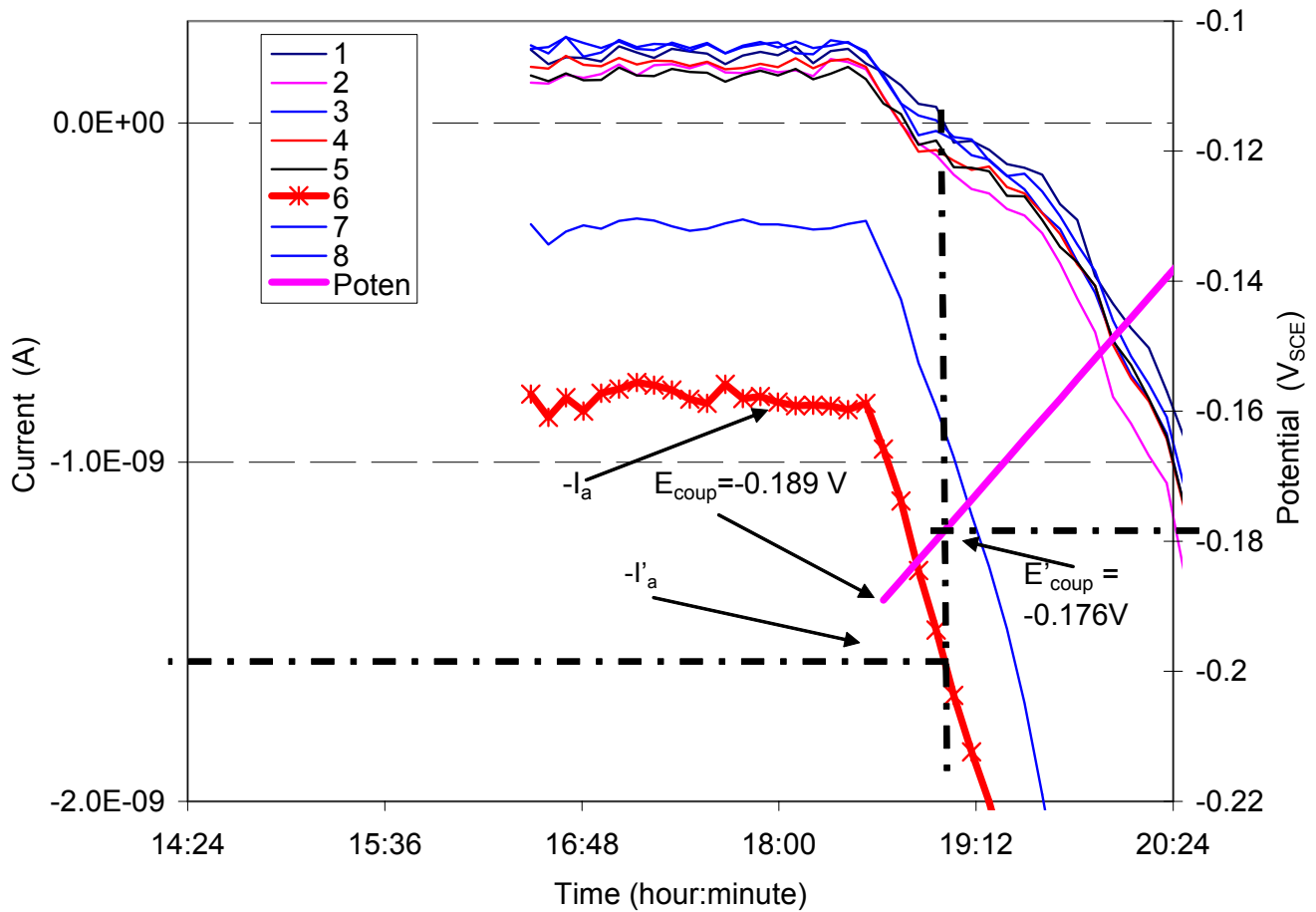


FIGURE 10. Response of the currents from the different electrodes in a Type 316 stainless steel MAS probe to the anodic potential scan in a 0.5 M NaCl solution

Note: Negative currents are anodic currents and positive currents are cathodic currents. The numbers in the legend denotes the identification numbers of the electrodes in the probe. Electrode #6 was the most anodic electrode before and after the potential scan.

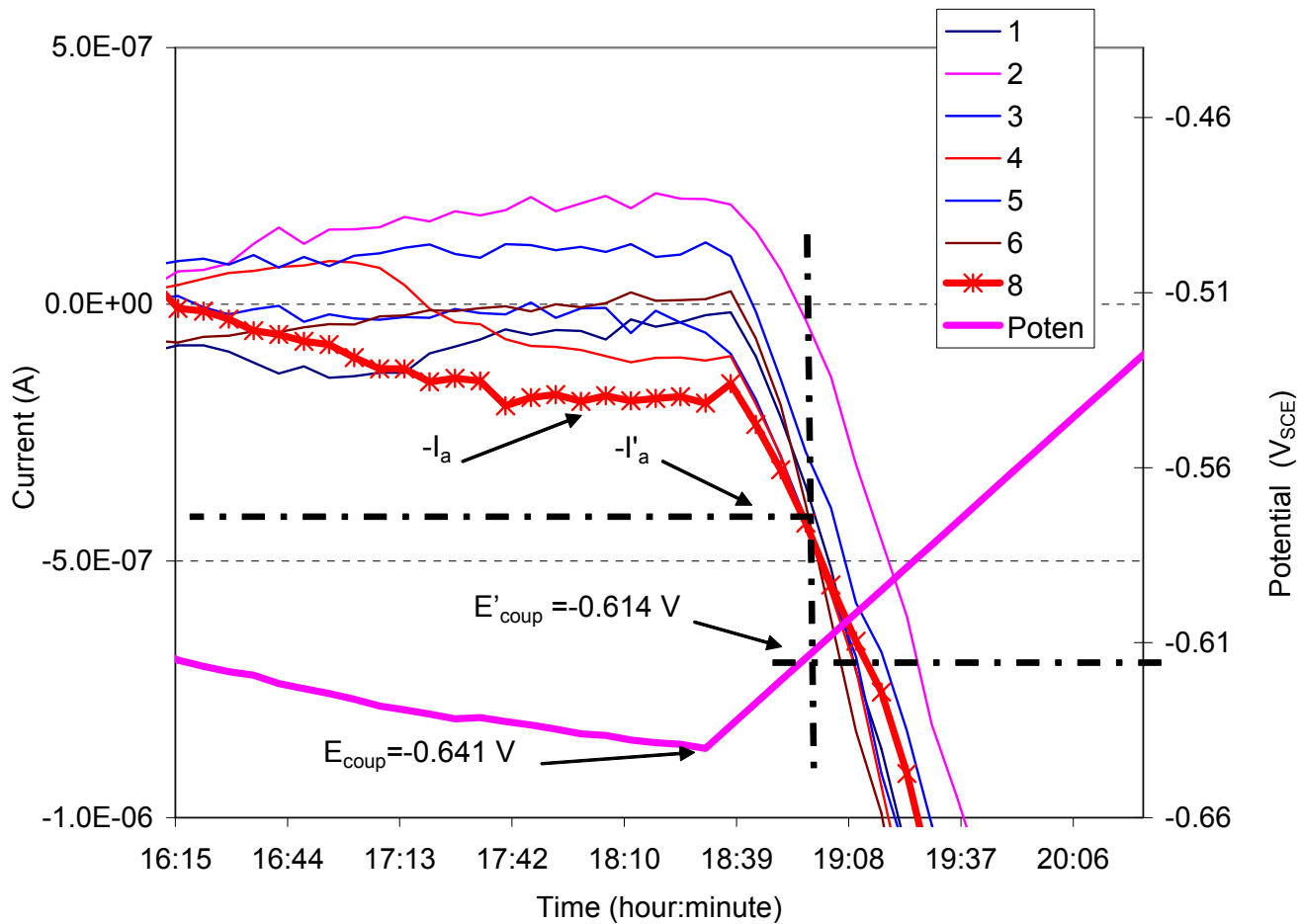


FIGURE 11. Response of the currents from the different electrodes of a Type 1008 carbon steel MAS probe to the potential change in a 0.5 M NaCl solution

Note: Negative currents are anodic currents and positive currents are cathodic currents. The number in the legend denotes the identification number of the electrodes in the probe. Electrode #8 was the most anodic electrode before the scan (at the natural coupling potential,  $E_{\text{coup}}$ ).

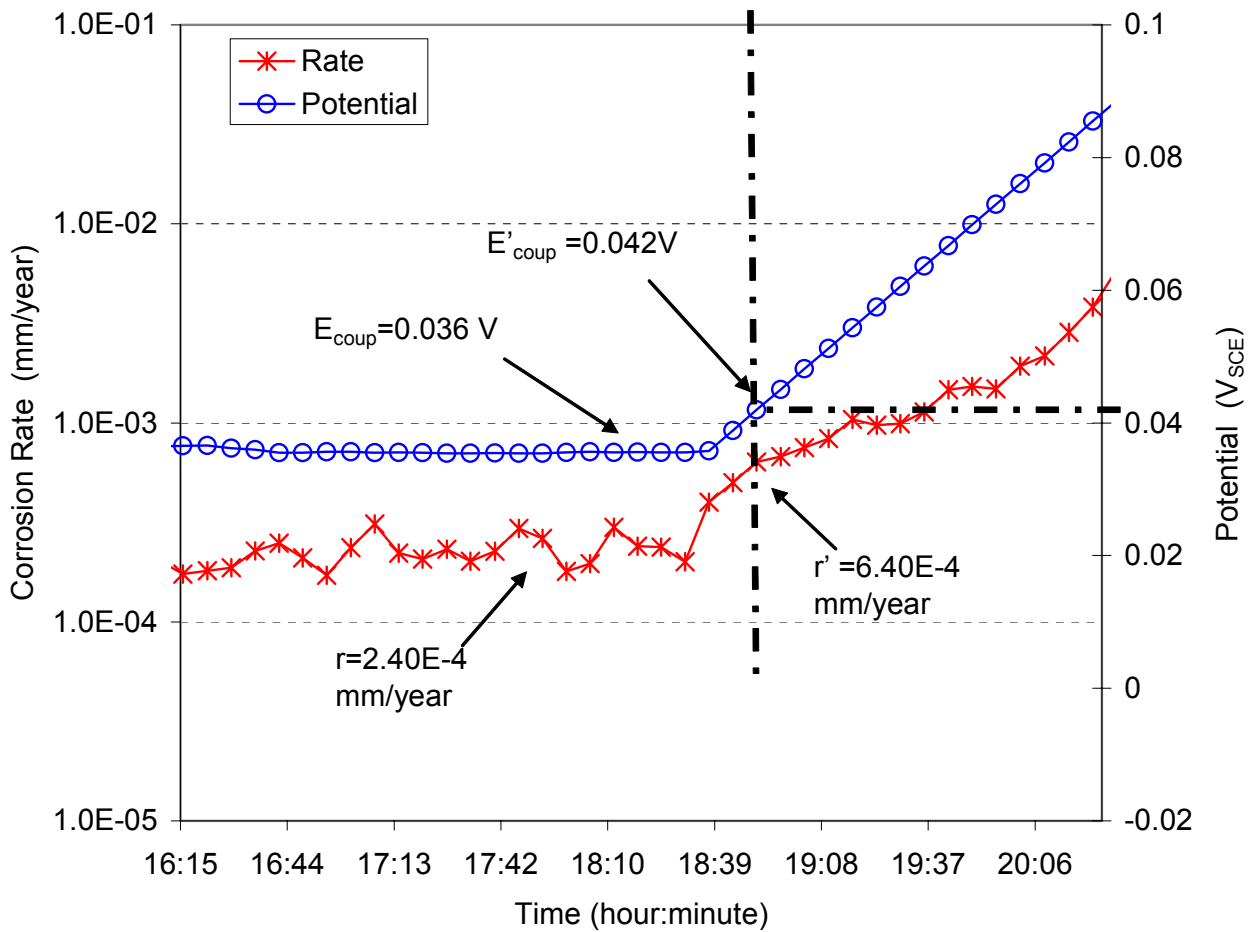


FIGURE 12. The corrosion rate of the Alloy 276 MAS probe derived from the most anodic electrode at natural coupling potential (Figure 9, Electrode #5). The corrosion rate,  $r' = 6.4 \times 10^{-4} \text{ mm/year}$ , is the upper bounding corrosion rate from the MAS probe.

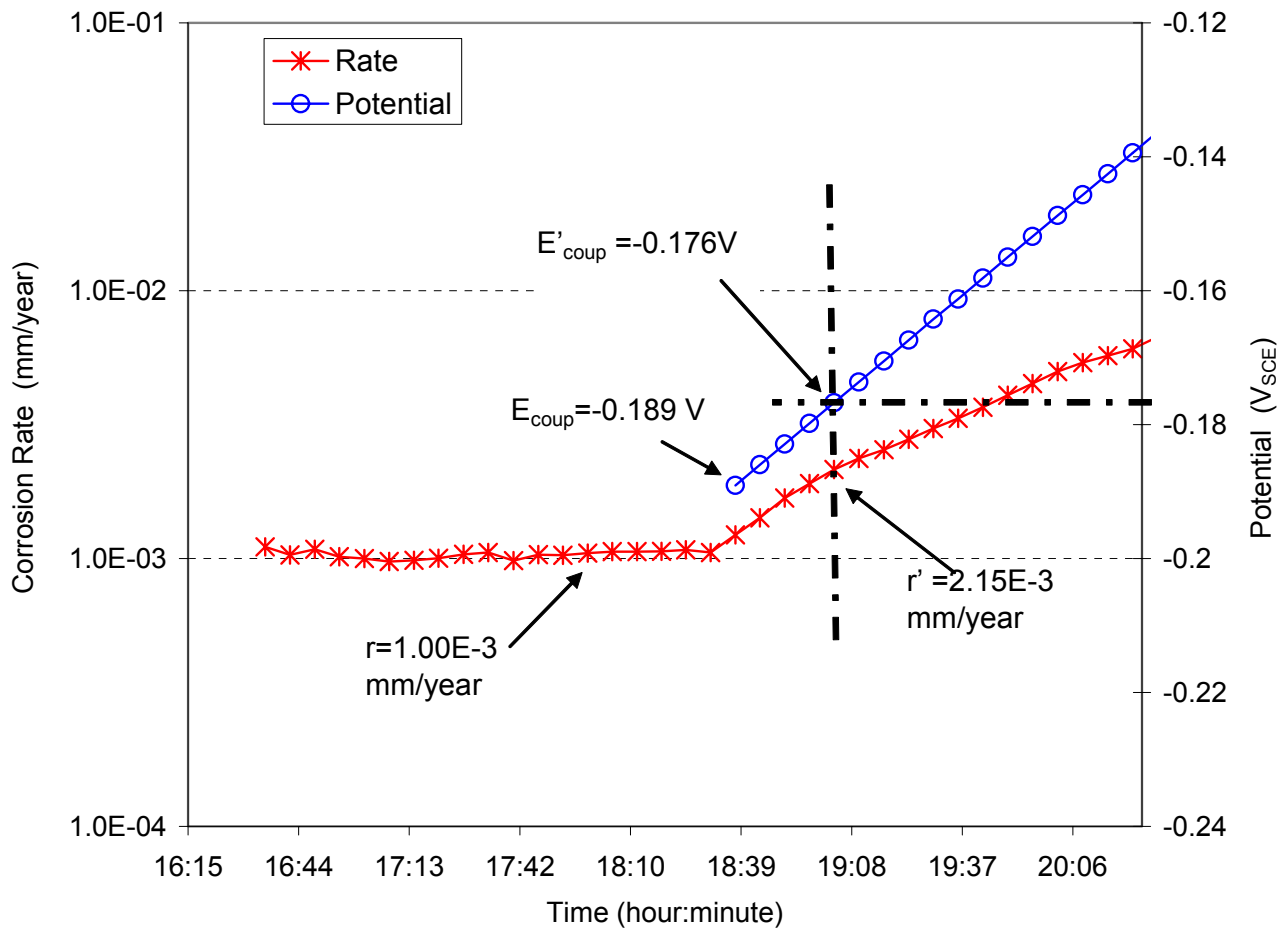


FIGURE 13. The corrosion rate of the Type 316 stainless steel MAS probe derived from the most anodic electrode at natural coupling potential (Figure 10, Electrode #6). The corrosion rate,  $r' = 2.2E-3$  mm/year, is the upper bounding corrosion rate from the MAS probe.

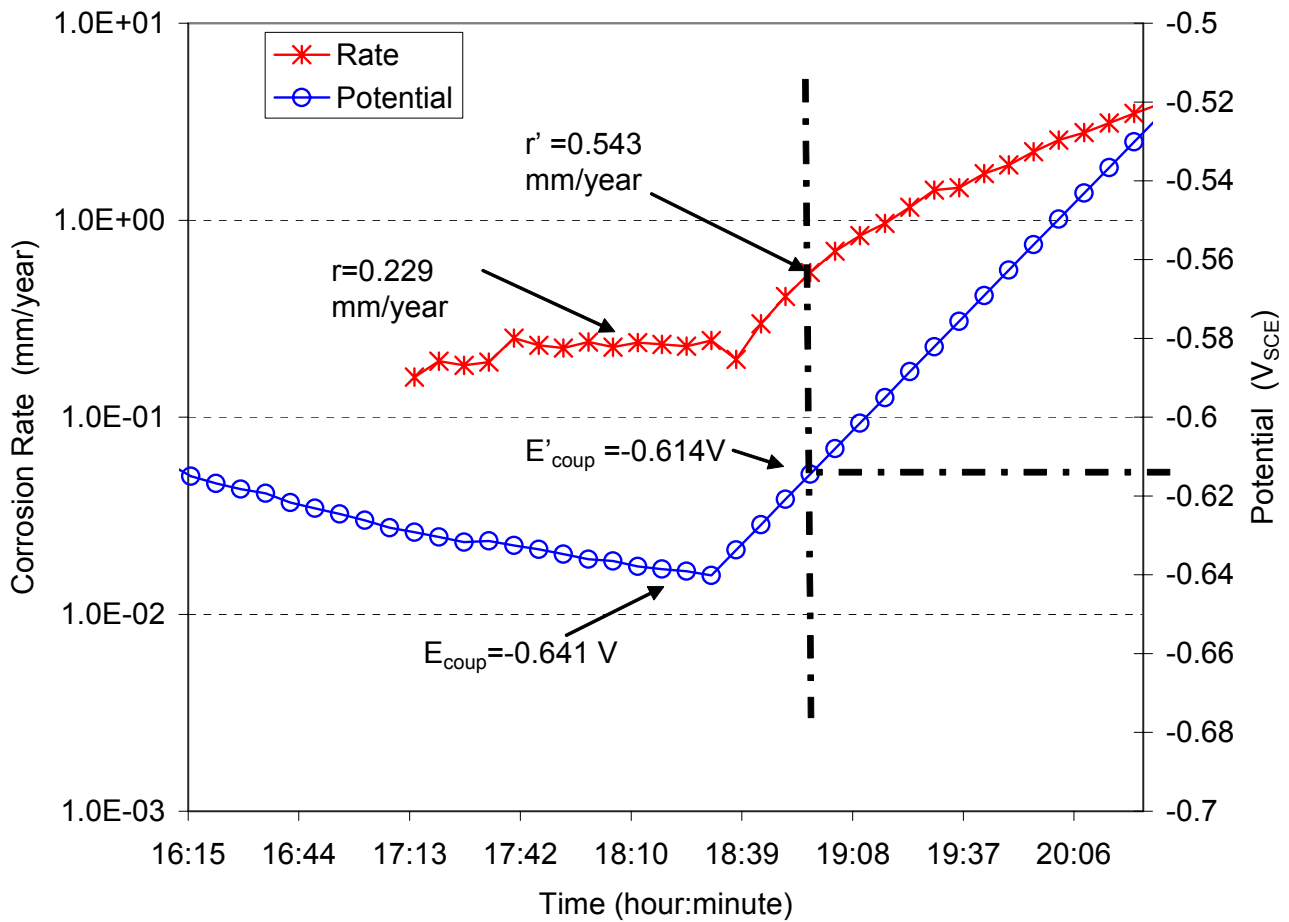


FIGURE 14 Response of the corrosion rate from the carbon steel MAS probe derived from the most anodic electrode at natural coupling potential (Figure 11, Electrode #8). The corrosion current,  $r' = 0.143$  mm/year is the upper bounding corrosion rate from the MAS probe.

FIGURE 1. Flows of electrons and currents among electrically isolated cathodic and anodic blocks on the surface of a corroding metal under localized corrosion conditions.  $I_a^{ex}$  and  $I_c^{ex}$  are the external anodic and cathodic currents, respectively.

FIGURE 2. Flow of electrons on a totally corroded active electrode as anode (a), a partially corroded electrode as anode (b), a passive electrode as cathode (c), and a partially corroded electrode as cathode (d) in a coupled MAS probe.

FIGURE 3. Schematic diagram of open-circuit electrode potentials for a cathodic electrode and an anodic anode, the natural and raised coupling potentials, and the dissolution currents of the anodic electrode at different coupling potentials in a MAS probe.

FIGURE 4. Typical open-circuit potentials measured from a coupled MAS probe made of Alloy 276 in a 0.5 M NaCl solution.

FIGURE 5. Typical open-circuit potentials measured from a coupled MAS probe made of Type 316 stainless steel in a 0.5 M NaCl solution

FIGURE 6. A proposed system that measures the corrosion rate using a coupled MAS probe at a raised coupling potential

FIGURE 7. Potential applied by a potentiostat to the coupling joint of the MAS probes during a preliminary demonstration test using the improved method

FIGURE 8. Responses of the currents from an eight-electrode MAS probe made of Alloy 276 to the potential changes as shown in Figure 7 in a 0.5 M NaCl solution

FIGURE 9. Response of the currents from the different electrodes in an Alloy 276 MAS probe to the anodic potential scan in a 0.5 M NaCl solution

FIGURE 10. Response of the currents from the different electrodes in a Type 316 stainless steel MAS probe to the anodic potential scan in a 0.5 M NaCl solution

FIGURE 11. Response of the currents from the different electrodes of a Type 1008 carbon steel MAS probe to the potential change in a 0.5 M NaCl solution

FIGURE 12. The corrosion rate of the Alloy 276 MAS probe derived from the most anodic electrode at natural coupling potential (Figure 9, Electrode #5). The corrosion rate,  $r' = 6.4E-4$  mm/year, is the upper bounding corrosion rate from the MAS probe.

FIGURE 13. The corrosion rate of the Type 316 stainless steel MAS probe derived from the most anodic electrode at natural coupling potential (Figure 10, Electrode #6). The corrosion rate,  $r' = 2.2E-3$  mm/year, is the upper bounding corrosion rate from the MAS probe.

FIGURE 14 Response of the corrosion rate from the carbon steel MAS probe derived from the most anodic electrode at natural coupling potential (Figure 11, Electrode #8). The corrosion current,  $r' = 0.143$  mm/year is the upper bounding corrosion rate from the MAS probe.